Limited Power Control of a Grid Connected Photovoltaic System

P Bala Sai Kiran

A Thesis Submitted to
Indian Institute of Technology Hyderabad
In Partial Fulfillment of the Requirements for
The Degree of Master of Technology

भारतीय प्रौद्योगिकी संस्थान हैदराबाद
Indian Institute of Technology Hyderabad

Department of Electrical Engineering

June 2015

Declaration

I declare that this written submission represents my ideas in my own words, and where ideas or words of others have been included, I have adequately cited and referenced the original sources. I also declare that I have adhered to all principles of academic honesty and integrity and have not misrepresented or fabricated or falsified any idea/data/fact/source in my submission. I understand that any violation of the above will be a cause for disciplinary action by the Institute and can also evoke penal action from the sources that have thus not been properly cited, or from whom proper permission has not been taken when needed.
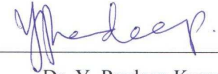
P. Bala Sai Kiran

(Signature)

_____

(P Bala Sai Kiran)

_____

(Roll No. EE12M1024)

Approval Sheet

This thesis entitled Limited Power Control of a Photovoltaic System Connected to Grid by P Bala Sai Kiran is approved for the degree of Master of Technology from IIT Hyderabad.

Dr. Y. Pradeep Kumar
Dept. of Electrical Engineering
Examiner-1

Dr. Raja Benerjee
Dept. of Mechanical and Aerospace Engineering
Examiner-2 (External)

Dr. Vaskar Sarkar
Dept. of Electrical Engineering
Adviser

Dr. K. Siva Kumar
Dept. of Electrical Engineering
Chairman

Acknowledgements

Dedication

my supervisor

Abstract

The objective of this thesis is to improve the performance of limited power point tracking (LPPT) of photovoltaic plants. Limited power point tracking refers to the control of power output from a photovoltaic array at a level below the maximum power point. The limited power point tracking exhibits advantages over maximum power point tracking (MPPT) both in terms of economy and system security. The previously reported LPPT methods, however, exhibit more oscillations at low power levels or require additional mode changing action under power scarcity and may malfunction under the rapidly varying environmental conditions. To avoid these difficulties, two novel LPPT control schemes are proposed. Both the schemes are carefully designed with minimum deviation from the traditional MPPT control so as to ensure easy implementation. Each of the controllers proposed has its own merit. The LPPT control under the proposed schemes can be implemented without the support of any local energy storage. Detailed case studies are performed to verify the effectiveness of proposed LPPT controllers. Additionally, in this thesis, performance of LPPT control of a single-stage, three-phase, grid connected photovoltaic system is studied.

Contents

List of Figures

List of Tables

Chapter 1

Introduction

As the penetration of the photovoltaic power into the grid is increasing day by day, it is important for photovoltaic systems to help grid support functions that are traditionally performed by rotating machines. The maximum power point tracking (MPPT) is most efficient technique for grid connected photovoltaic systems. However, if the grid connected inverters continue to operate in maximum power point tracking mode, the following issues may arise [1].

- Overloading of the grid at peak power generation, which may induce over voltages.

- Limited utilization of photovoltaic inverter.

- High temperature peaks and variations on switching devices due to intermittency, which accelerates the degradation of the switching devices.

To handle this overloading issue, there are some possible solutions given in the literature [2]:

1. storing the additional energy;

2. reducing the secondary LV transformer voltage adjusting tap;

3. installing auto transformers and voltage regulators;

4. allowing the distributed generation systems (DGs) to absorb the reactive power;

5. expanding the grid infrastructure (increase the conductor size and transformer rating);

6. curtailing some photovoltaic units, which will reduce the power.

The main limitation of the first technique is that energy storage is quite expensive for high power capacity and it requires a continuous maintenance activity. Frequently, tap changing is also not possible. Installation of auto transformers and voltage regulators introduces unreliability factor into the system. Reactive power control of DGs results in higher currents and losses in the distributed network (in the distributed network, voltage is less susceptible to reactive power due to high resistance). Grid expansion is also a costly approach.

Since the aforementioned solutions introduce considerable investment, several hybrid control concepts have been suggested in the previous research. In order to allow more flexible operation of the system, the active power control or LPPT of photovoltaic plants is emerging out as a new

technology [3]. Under the limited power point tracking (LPPT) control, the photovoltaic system is operated in a way so that any specified amount of power, subjected to maximum power availability constraint, can be extracted from the photovoltaic array. In the case of the power requirement specified (through a power reference command) is more than the maximum available power. The power output of the photovoltaic array should settle down to the maximum power point (MPP). Some of the shortcomings of LPPT control techniques proposed in the literature are supplementary observer system, local energy storage and oscillations in the power tracking.

With a motivation to improve the performance of limited power point tracking, a couple of novel LPPT control schemes are proposed in this thesis. The performance improvement is claimed, specifically, in the form of reduced power oscillation over a wide range of operating conditions without compromising with the settling time. In this thesis, the photovoltaic array is considered to be connected to a voltage controlled DC bus through a DC-DC converter. The present application of the LPPT control is aimed only at periodic scheduling of the photovoltaic power output. Similarly to [4], the methodologies proposed do not require any local energy storage support or separate MPPT controller, and can work under the rapidly varying environmental condition. The foundation of both the schemes is the deployment of variable perturbation step size, which is suitably adapted for the limited power point tracking control. The schemes proposed exhibit certain superiorities against each other. This thesis also presents a study on the LPPT control of single-stage, three-phase grid connected photovoltaic system. In the case of a single-stage photovoltaic system, the photovoltaic array is directly interfaced with the grid through a DC-AC converter.

1.1   Organization of This Thesis

This chapter gives an introduction of limited power concept and organization of the thesis.

Chapter 2: This chapter covers the literature survey of grid connected photovoltaic systems, standards, MPPT techniques, scope of LPPT and existing LPPT techniques and reviews the mathematical modelling and characteristics of a photovoltaic array.

Chapter 3: In this chapter, two novel schemes are proposed to track the limited power. Detailed case studies are performed to verify the effectiveness of proposed LPPT controllers.

Chapter 4: In this chapter, the performance of LPPT control of a single-stage photovoltaic system is investigated. Detailed simulation and experimental, studies are performed to verify the potentiality of LPPT control in single-stage photovoltaic power conversion.

Chapter 5: This chapter concludes the thesis and discusses the possible future scopes of work.

Chapter 2

Literature Review

This chapter consists of a brief literature survey, which covers the various grid connected photo-voltaic system configurations, MPPT algorithms, LPPT algorithms and mathematical modelling of photovoltaic cell/array. Nowadays, the concept of distributed energy (DG) is gaining popularity due to economic, technical and environmental benefits. Normally, high capacity photovoltaic systems are connected to the grid at sub transmission voltage levels. However, such photovoltaic systems are growing in the distributed networks.

2.1 Photovoltaic Cell Modelling

There are two different models of a photovoltaic cell that can be found in literature [5]. Those are double diode and single diode models. In this thesis, single diode model is considered, which is shown in the Fig. 2.1 [5]–[8]. Based upon the equivalent circuit representation, the V-I equation of
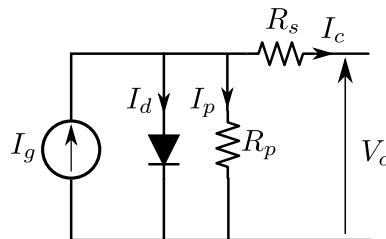
Figure 2.1: Single diode equivalent circuit of a photovoltaic cell.

a photovoltaic cell can be derived as follows.

$$I_c = I_g - I_o \left(e^{\frac{\beta(V_c + R_s I_c)}{A}} - 1 \right) - \left(\frac{V_c + R_s I_c}{R_p} \right) \tag{2.1}$$

where, β is the inverse thermal voltage, A is diode ideality factor. It's value usually the value between 1 and 2.5. The inverse thermal voltage is defined as follows.

$$\beta = \frac{q}{KT} \tag{2.2}$$

in the above equation, q $(= 1.6 \times 10^{-19}$ C) is electron's charge, K $(= 1.38 \times 10^{-23}$ J/K) is Boltzmann's constant, and T is junction temperature (Kelvin). The current generated by photovoltaic cell (I_g) depends on temperature and irradiance G (W/m^2).

$$I_g = [I_{scr} + K_i\,(T - T_r)]\,\frac{G}{G_r} \tag{2.3}$$

where, I_{scr} is short circuit current at the reference condition is also referred to as standard test condition (STC), which corresponds to the irradiance level of 1 W/m^2 and temperature 25^0 C. K_i is current temperature coefficient (A/K), G_r and T_r are reference irradiance and reference temperature. Diode reverse saturation current (I_0) depends only on the temperature.

$$I_0\,(T) = \frac{I_{scr} + K_i\,(T - T_r)}{\mathrm{e}^{\frac{\beta}{A}(V_{ocr} + K_v(T - T_r))} - 1} \tag{2.4}$$

where, K_v is voltage temperature coefficient (V/K), V_{ocr} is open circuit voltage at STC.

2.1.1   Photovoltaic Array Modelling

Individual photovoltaic cells are organized in series-parallel combination to form photovoltaic array with necessary voltage level and power production capacity. The equivalent circuit representation of photovoltaic array is similar to equivalent circuit of photovoltaic cell; only the difference is parameters are suitably modified by taking into account the number of series cells and parallel strings. The basic characteristics of photovoltaic cell is shown in Fig. 2.2 and Fig. 2.3. Fig. 2.2 shows power vs. voltage characteristics of a photovoltaic system, where P_{mpp} is maximum power point (MPP), V_{mpp} is voltage at MPP and V_{oc} is open circuit voltage. Fig. 2.3 shows current vs. voltage characteristics of a photovoltaic system, where I_{mpp} is current at maximum power and I_{sc} is short circuit current. In the modelling of photovoltaic array, photovoltaic cell parameters are scaled according to the following equations.

$$I_g^a = N_p I_g \tag{2.5}$$

$$R_p^a = \frac{N_s}{N_p} R_p \tag{2.6}$$

$$R_s^a = \frac{N_s}{N_p} R_s \tag{2.7}$$

$$A^a = N_s A \tag{2.8}$$

$$K_i^a = N_p K_i \tag{2.9}$$

$$K_v^a = N_p K_v \tag{2.10}$$

$$I_0^a = N_p I_o. \tag{2.11}$$
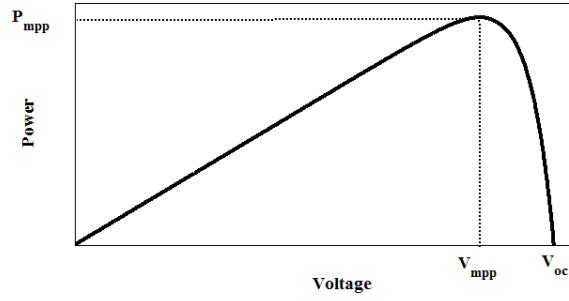
Figure 2.2: Basic power vs. voltage characteristics of a photovoltaic cell/photovoltaic array.
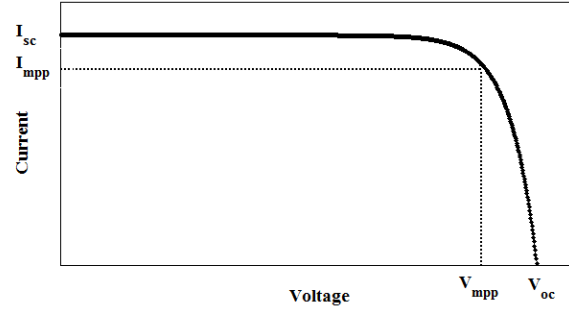
Figure 2.3: Basic current vs. voltage characteristics of a photovoltaic cell/photovoltaic array.

2.2 Classification of Grid Connected Photovoltaic System Configurations

Grid connected photovoltaic system can be classified based on the number of stages of energy conversion, isolation and type of grid interface [9]. Based on the number of power conversion stages, photovoltaic systems are classified into two types, one is single stage power conversion and other one is dual stage power conversion. In the dual stage power conversion, the voltage amplification and MPPT are handled by the DC-DC converter and DC link voltage controlled by the inverter. A Dual stage topology is shown in Fig. 2.4(b). In case of a single stage operation, voltage amplification, MPPT and DC link voltage control are handled only by a DC-AC converter. Fig. 2.4(a) shows a single phase configuration. Single stage configuration has high efficiency and reliability compared to dual stage configuration.

Depending on the nature of isolation, the inverters can be classified into two types; i) isolated ii) non-isolated. Normally, isolation is provided by using a transformer. The transformer isolation is provided depending upon country's Electricity Regulation Act. In UK and Italy, isolation is a prerequisite. Isolation can be provided by using line frequency transformer [shown in Fig. 2.5 (a)] or by using a high frequency transformer which is embedded in DC-DC converter [shown in Fig. 2.5 (b)]. In some countries, like Spain and Germany, isolation is excluded. The disadvantage of non-isolated system is that it will inject DC current into the grid.

Grid connected inverters can also be classified based on the converter type such as, 1. voltage source inverters (VSI) 2. current source inverters (CSI) 3. Z- source inverters. Normally, VSI is preferred over CSI.
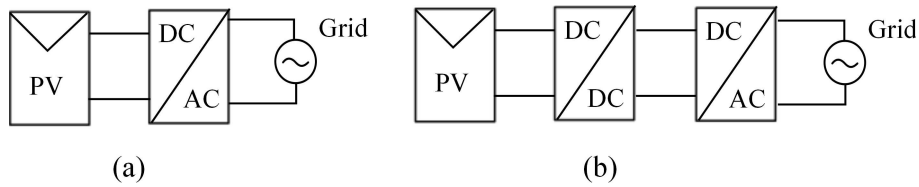
Figure 2.4: Power conversion of photovoltaic system based on the number of stages. (a) Single stage power conversion system; (b) dual stage power conversion system.
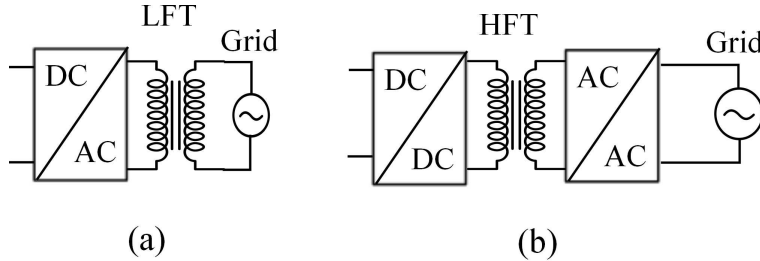
Figure 2.5: Transformer embedded inverter solutions. (a) Line frequency transformer is embedded between the grid and the inverter; (b) high frequency transformer embedded in DC to DC converter.

2.3 Standards Dealing with Interconnection of Photovoltaic Systems to Grid

The inverter interfacing the photovoltaic array to the grid perform two tasks: (i) to ensure that photovoltaic system is operated at its MPPT. (ii) to inject the sinusoidal current to the grid at the desired power factor.

Grid connected inverter should follow some standards according to IEC61727, IEEE1547 and EN61000-3-2 [10]. Standards deal with power quality and island detection. Summary of the standards presented in Table. 2.3. From the protection point of view, islanding detection is a major task with regard to the operation of an inverter. Islanding refers to sudden loss of grid connection in a grid connected microgrid. The islanding can be scheduled or unintentional. Intentional islanding happens due to sudden faults. In practice, two types of islanding detection methods are there, namely, passive methods and active methods [10]. Passive methods continuously observe the deviation in the grid parameters (voltage and frequency) when the grid connection is lost. Active methods inject some disturbance into the grid, and monitor the effect. Active methods affect the power quality, but passive methods do not. IEEE and IEC standards kept limit on DC current injection into the grid; otherwise, DC component of the current may saturate the transformers.

2.4 MPPT Algorithms for Photovoltaic System

MPPT is the most popular technique for the operation of grid connected photovoltaic systems. It will extract maximum power from the photovoltaic system at all the environmental conditions. The popular MPPT techniques are hill climbing or perturb and observe (P&O), incremental conductance method. Reference [11], [12] reviews the different MPPT algorithms introduced since 1968.

Table 2.1: Summary of the standards dealing with grid-connected photovoltaic systems

ISSUE	IEC61727	IEEE1547	EN61000-3-2
Nominal power	10 kW	30 kW	16×230=3.7 kW
Harmonic currents Order h limits	(3-9)4.0% (11-15) 2% (17-21) 1.5% (23-33)0.6%	(2-10)4.0% (11-16)2.0% (17-22)1.5% (23-34) 0.6% (>35)0.3%	(3)2.30 A (5) 1.14 A (7) 0.77 A (9) 0.40 A (11) 0.33 A (13)0.21 A (15-39)2.25/h
Maximum current THD	5 %	5 %	
Power factor at 50 % rated power	0.9		
DC current injection	Less than 1% of rated output current	Less than 0.5% of rated output current	< 0.22 A corresponds to a 50 W half wave rectifier

2.4.1 Perturb and Observe Method

Flow chart of perturb and observe algorithm is shown in Fig. 2.6. In this method, the reference voltage varies with steps of δV based on the sign of dP ($P_{pv}[n] - P_{pv}[n-1]$) and dV ($V_{pv}[n] - V_{pv}[n-1]$). If both signs are positive, the reference voltage (v_{ref}^r) increases, otherwise decreases. The problem with this method is, it never tracks the true MPP, and it always oscillates around the MPP. In the case $V_{pv}[n] - V_{pv}[n-1]$ is zero, the respective term in denominator should be replaced with a small positive number.
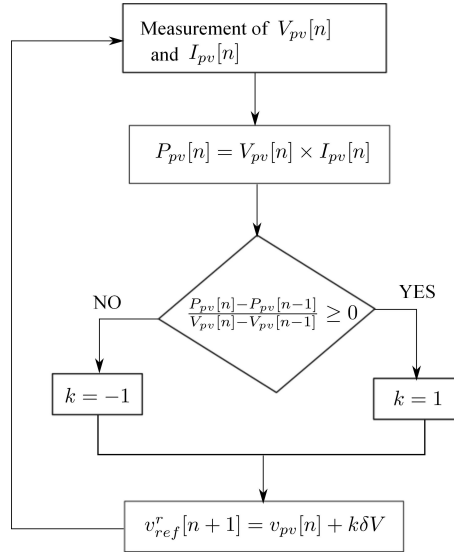
Figure 2.6: Flowchart of P&O algorithm.

2.4.2 Incremental Conductance Method

Incremental conductance method (INC) is developed based on the following equation.

$$\frac{di_{pv}}{dv_{pv}} + \frac{i_{pv}}{v_{pv}} = 0. \tag{2.12}$$

If $\left(\frac{di_{pv}}{dv_{pv}} + \frac{i_{pv}}{v_{pv}}\right)$ is positive, operating point is lies on left hand side of MPP on the P-V curve. If it is negative, operating point lies on right side of the MPP. Flow chart of incremental conductance method is shown in Fig. 2.7.
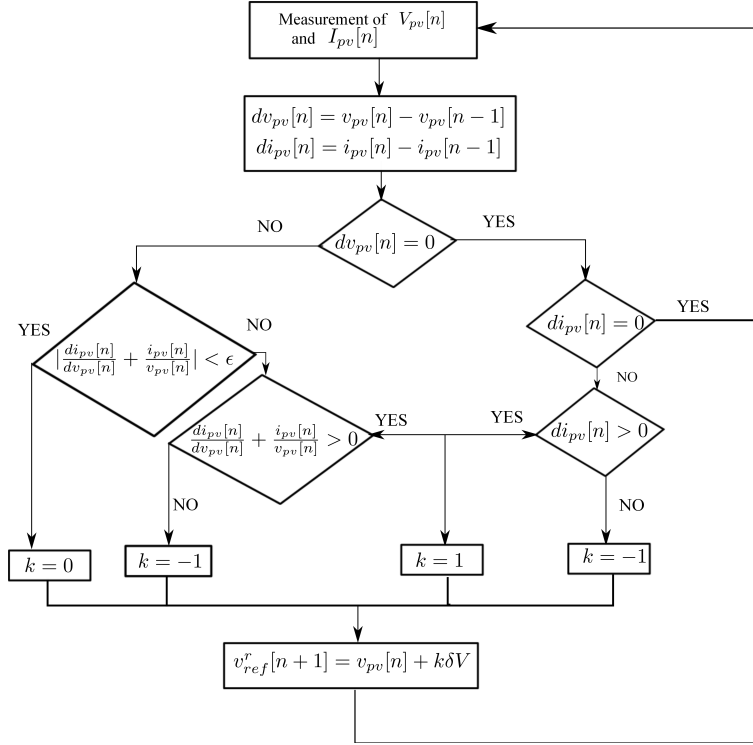
Figure 2.7: Flowchart of INC algorithm.

As in Fig. 2.7, if $\left(\frac{di_{pv}}{dv_{pv}} + \frac{i_{pv}}{v_{pv}}\right)$ is positive and larger than ϵ, voltage must be increased to reach the maximum power point. If $\left(\frac{di_{pv}}{dv_{pv}} + \frac{i_{pv}}{v_{pv}}\right)$ is negative and its absolute value is larger than ϵ, voltage is decreased by one step. Once $\left(\frac{di_{pv}}{dv_{pv}} + \frac{i_{pv}}{v_{pv}}\right)$ becomes in absolute value is less than ϵ, then the MPP has been reached.

2.5 LPPT Algorithms for Photovoltaic System

The MPPT is the conventional approach for operating the photovoltaic plants. The MPPT based operation of solar plants inevitably requires coordinated energy storage capacity or unconstrained evacuation of the excess power to the main grid. Alternatively, some auxiliary controllable load units are required to burn the excess power.

The LPPT control has several advantages over the conventional MPPT control in terms of economy, improvement of system frequency profile and increase of inverter life [1]–[14]. First of all, there is no stringent requirement to size energy storage devices strictly according to the installed photovoltaic plant capacity for maintaining generation and load balance. Relaxation of the particular

constraint, in turn, provides more flexibility to optimally construct a microgrid under the sanctioned budget. For a grid connected photovoltaic system, the power transfer to the main grid is to be limited in the case of the possibility of line overloading.

The concept of limited power point tracking is given in (2.13). If the given reference power is less than the maximum available power, the controller will track the reference power, else it will track the maximum power point.

$$P_{pv} = P_{ref} \text{ if } P_{ref} \leq P_{mpp} \quad (2.13)$$

$$= P_{mpp} \text{ if } P_{ref} > P_{mpp}. \quad (2.14)$$

In low voltage distributed networks, voltage mainly depends on active power rather than reactive power. In a highly penetrated grid connected photovoltaic system, overvoltage is the main problem. To avoid the overvoltage problem, droop based active power control scheme is proposed in [2], which is shown in Fig. 2.8. In this scheme, if the bus voltage (V) is greater than V_{cri}, reference power input to the inverter (P_{inv}) will decrease. If the bus voltage is less than the critical voltage, inverters transfers maximum power to the grid [2].

$$P_{inv} = P_{MPPT} - m(V - V_{cri}). \quad (2.15)$$
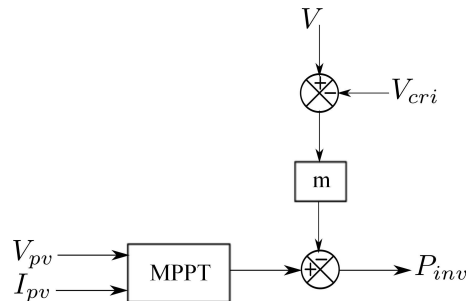
Figure 2.8: Droop based active power control.

In [1] and [13], a hybrid power control concept proposed for grid connected photovoltaic inverters. In this method, it is shown that operating a photovoltaic system with some margin from the maximum power point can increase the inverter life. The control architecture is shown in Fig. 2.9. In this method, if P_{pv} is less than P_{limit}, it will operate in the MPPT mode. In case P_{pv} is more than the P_{limit} it will operate in constant power mode.

In [14] and [15], it is shown that the MPPT control can degrade the system frequency for high penetration level of the solar power. Involvement of the photovoltaic sources in the dynamic load frequency control is also recommended in [4] and [16]. In [16], implementation of frequency regulation scheme for solar system proposed. This additionally requires automatic adjustment of the power reference command to the LPPT controller. For the respective operation of a photovoltaic plant, the LPPT control is necessary. The LPPT control of a bulk grid-connected photovoltaic plant also has strong implication in the context of power market that involves bid based scheduling of power production levels [14]. Apart from the photovoltaic plants, the LPPT control has also been proposed for wind generators [17]. There are already some LPPT control techniques proposed in literature
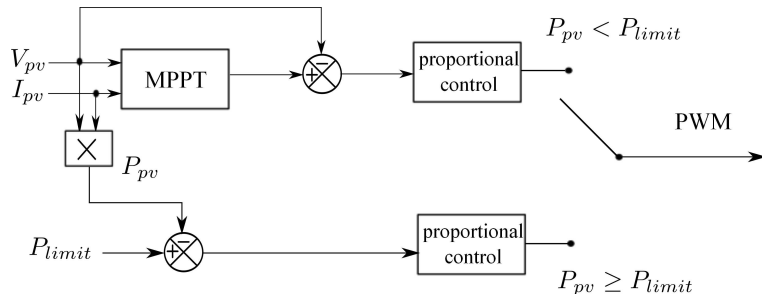
Figure 2.9: Hybrid power control.

[1]–[2]–[4], [13] –[22]. However, one common shortcoming of all the above techniques is that those may fail if the operating point accidentally moves to the other side (w.r.t. the side chosen for operation) of MPP on the P-V curve.

The control architectures proposed in [1], [18]–[20] require separate MPPT and LPPT controllers. The LPPT controllers proposed there cannot detect the maximum power limit of the photovoltaic plant; therefore, explicit mode changing action is required in the case of power scarcity. For [1], [18] and [22] an additional observer system is required to continuously monitor the maximum available power level so as to switch from the LPPT mode to the MPPT mode whenever required. The requirement for the online monitoring of maximum available power increases the system cost and makes the system vulnerable to the inaccuracy and time gap in the maximum power point calculation. In the case of [19], current references generated by MPPT and LPPT controllers are compared and the controller that commands lower current level is selected to decide the mode of operation. In [20], a hysteresis controller is used for mode changing based upon the measurement of DC link voltage. The control architecture proposed here, however, requires the support of local energy storage since the reference power command is provided to the DC-AC converter. The LPPT control techniques proposed in [1], [18]–[21] may fail if the operating point accidentally moves to the other side (w.r.t. the side chosen for operation) of MPP on the power versus voltage curve. This may be caused by the rapidly varying environmental condition. The consequence can be either system instability or wrong trapping of the operating point at MPP. The methodology proposed in [16] uses an approximate linear relationship between power and voltage, which is similar to the fractional open circuit voltage or short circuit current methodology for maximum power point tracking. Therefore, the exact tracking of the specified reference power level is not possible. The limited power point tracking methodology proposed in [4] is, however, free from all the above burdens and is generally practicable. However, there may be huge oscillations while tracking a low power level. For the methodology proposed in [4], the DC voltage control is performed by the DC-AC converter, whereas, the power reference command is provided to the DC-DC converter. The reference power level is tracked by means of a modified P&O approach with fixed perturbation step size. Separate MPPT controller is not required in this case. However, because of the extremely high and monotonically increasing slope of the P-V curve in the LPPT zone, very small perturbation step size is required for the stable tracking of the power reference. Otherwise, huge oscillations can be observed at low power levels. A conservative choice of the perturbation step size (at a very low value), on the other hand, makes the system response sluggish especially at the high power and low irradiance levels.

Chapter 3

Limited Power Tracking of a Photovoltaic Plant Connected across Voltage-Controlled DC Bus

This chapter presents two novel schemes to improve the performance of LPPT. The LPPT control techniques proposed are verified through hardware-in-loop simulation for a dual-stage photovoltaic system.

3.1   Basic LPPT Control

The principle of LPPT control of a photovoltaic system is explained with the help of the P-V curve shown in Fig. 3.1. Here, Point M indicates the maximum power point. The maximum power availability is indicated by P_{mpp}. Corresponding to the power reference command $P_{ref,1}$, which is less than P_{mpp}, there can be two possible operating points, B and E. Point B corresponds to low voltage operation, whereas, point E corresponds to high voltage operation. The LPPT operation (at equilibrium) is to be confined to only one particular side of MPP on the P-V curve. Operation on the right hand side is preferable (i.e., Point E for the above case) since the higher operating voltage leads to lower power loss. The dynamics of the system operating point for the reference power $P_{ref,1}$ is shown by the black arrows. For any of the intermediate Operating Points A, B and C, which lies on the left side of MPP, the voltage output of the photovoltaic array is to be further increased. Also for the intermediate operating point M or D (which does not lie on the left side of MPP), the output voltage is to be driven higher since the present output power level is higher than the reference power level. However, a reduction in the photovoltaic array output voltage is required if the system is presently operating at F. This is because, point F is located on the right hand side of MPP and provides lower power output compared to $P_{ref,1}$. In the case of the reference power command $P_{ref,2}$, which is higher than P_{mpp}, the operating point should follow the same dynamics as for MPPT. This is shown by red arrows in Fig. 3.1.

The input to the duty-ratio controller (Fig. 3.2) is provided by a voltage reference generator, which is a discrete-time system. The dynamics of the voltage reference generator is governed by the
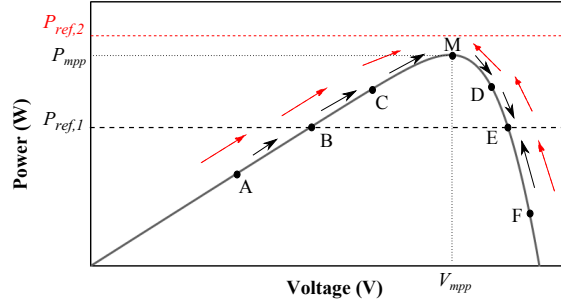
Figure 3.1: Depiction of LPPT control.

following difference equation.

$$V_{pv,ref}[n] = V_{pv,ref}[n-1] - \sigma[n]\Delta V. \tag{3.1}$$

Here, n indicates the sampling time instant and ΔV is the step size for voltage correction. The
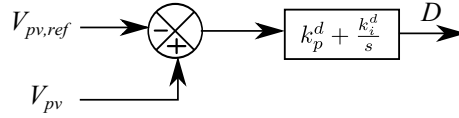
Figure 3.2: Duty ratio controller.

directional factor σ for voltage correction decides whether to increase or decrease the reference voltage for the duty ratio controller. The value of σ at the nth time instant is determined through the following equation.

$$\begin{aligned}
\sigma[n] &= 1 \quad \text{if} \quad \Gamma[n] \leq 0 \text{ and } P_{pv}[n] - P_{ref} < -\epsilon \\
&= 0 \quad \text{if} \quad |P_{pv}[n] - P_{ref}| \leq \epsilon \\
&= -1 \quad \text{otherwise.}
\end{aligned} \tag{3.2}$$

Here, ϵ represents the tolerance band for convergence. Index Γ determines the location of the present operating point with respect to MPP. The particular location monitoring index can be calculated by employing the P&O or INC principle as follows.

$$\begin{aligned}
\Gamma[n] &= \frac{V_{pv}[n]I_{pv}[n] - V_{pv}[n-1]I_{pv}[n-1]}{V_{pv}[n] - V_{pv}[n-1]} \quad \text{for P\&O} \\
&= \frac{I_{pv}[n]}{V_{pv}[n]} + \frac{I_{pv}[n] - I_{pv}[n-1]}{V_{pv}[n] - V_{pv}[n-1]} \quad \text{for INC.}
\end{aligned} \tag{3.3}$$

In principle, positive and negative values of Γ indicate locations on the left hand side and right hand side, respectively, of MPP on the P-V curve. At MPP, Γ should be zero. It is obvious that removal of the conditions [from (3.2)] associated with P_{ref} converts the LPPT control into the MPPT control. The LPPT control scheme proposed in [4] is, in effect, derived from the conventional MPPT control with fixed perturbation step size. The particular control scheme will be referred to as fixed step LPPT (FSLPPT) control in the subsequent sections.

3.2 Proposed LPPT Control Schemes

Two novel LPPT control schemes are proposed. The FSLPPT control may impose serious compromise between the response time and the power oscillation. To mitigate this issue, an LPPT control scheme is developed with dynamic adjustment of the perturbation step size. This is in line of the variable step MPPT control [23]; but, the step size adjustment is to be carried out with specific focus on the LPPT application. In the other scheme proposed, the concept of variable step is converted into the concept of variable rate through the use of a continuous-time controller for the voltage reference generation. The control schemes proposed are, thus, referred to as variable step LPPT (VSLPPT) control and variable rate LPPT (VRLPPT) control, respectively.

3.2.1 VSLPPT Control

The basic architecture of the VSLPPT control is similar to that of the FSLPPT control. However, the dynamics of the voltage reference generator is now governed by the following equation.

$$V_{pv,ref}[n] = V_{pv,ref}[n-1] - \sigma[n]\alpha[n]\Delta V. \tag{3.4}$$

The value of the step adjustment factor α depends upon the proximity to the reference power point
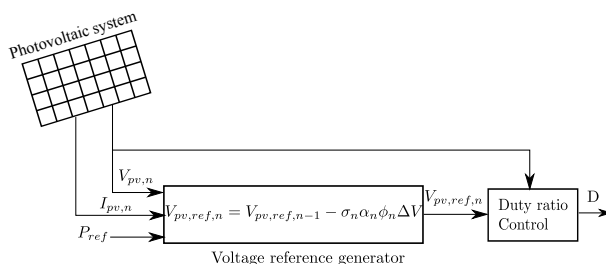
Figure 3.3: Schematic diagram of VSLPPT control.

as well as on the present location of the operating point on the P-V curve with respect to MPP. So long as the operating point is on the left hand side of MPP, the perturbation step size does not need to be varied. This is because, in order to track a power level below the maximum power, the operating point should, anyhow, be first shifted to the right hand side of MPP. On the right hand side of MPP, α can be kept proportional to the absolute value of the difference between the reference power and the measured power. However, there must be some upper limit on α. Otherwise, the system response may be highly oscillatory if the initial operating point on the right hand side of MPP is far away from the reference power point. This particularly affects the MPPT mode of operation and may result in huge power oscillations if the maximum available power suddenly falls below the power reference because of the sudden variation in environmental conditions. The value of α at the nth time instant can, therefore, be determined as follows. In this thesis, the performance of LPPT control of a single-stage photovoltaic system is investigated. Detailed simulation and experimental studies are performed to verify the potentiality of LPPT control in single-stage photovoltaic power conversion.

$$\begin{aligned} \alpha[n] &= 1 \ \text{if} \ \Gamma[n] > 0 \\ &= \min\{1, \gamma|P_{pv}[n] - P_{ref}|\} \ \text{if} \ \Gamma[n] \leq 0. \end{aligned} \tag{3.5}$$

Alternative forms of the step size adjustment can also be explored. The base voltage step size ΔV, sampling frequency and duty ratio controller parameters can be tuned based upon the MPPT mode of operation. Those parameters are similar to their counterparts in the traditional MPPT control. Therefore, additional effort is required only for tuning the step adjustment constant of proportionality γ based upon the LPPT operation.

In addition to employing variable perturbation step size, it is also useful to have a power scarcity indicator for minimizing power oscillations during the MPPT mode of operation. The value of the power scarcity indicator (symbolized as ϕ) at the nth time instant can be calculated as follows.

$$\begin{aligned} \phi[n] &= 0 \ \text{if} \ |\Gamma[n]| \leq \epsilon \ \text{and} \ P_{pv}[n] \leq P_{ref} \\ &= 1 \ \text{otherwise.} \end{aligned} \tag{3.6}$$

The occurrence of zero value of ϕ indicates power scarcity. It is also meaningful to define the convergence band around the reference power point in proportion to the reference power level. The modified convergence criterion in voltage correction, therefore, appears as follows. the expression of the voltage change direction detector σ is shown in (3.7).

$$\sigma[n] = 0 \ \text{if} \ \phi[n] = 0 \ \text{or} \ |P_{pv}[n] - P_{ref}| \leq \mu P_{ref}. \tag{3.7}$$

The convergence band constant of proportionality for the reference power point is indicated by μ.

3.2.2 VRLPPT Control

In principle (i.e., based upon the steady-state model of the DC-DC converter), it should be possible to improve the VSLPPT control performance by reducing the base voltage step size (i.e., ΔV) along with suitably increasing the sampling frequency of the voltage reference generator. However, with a high sampling frequency, the location detection of the steady operating point corresponding to the present reference voltage output may be incorrect because of the transients in the DC-DC converter. Therefore, an alternative control strategy can be to separate out the location and convergence detection component from the voltage reference generator. The sampling frequency of the location/convergence detection module can be set in the traditional manner (for example, according to the MPPT control performance). However, the voltage reference generator can now run at arbitrarily high sampling frequency. In the limiting case, the sampling frequency of the voltage reference generator can be made infinitely high. Therefore, the voltage reference generator, effectively, turns into a continuous-time system. This leads to the concept of VRLPPT control.

The schematic arrangement of the VRLPPT control is shown in Fig. 3.4. The location of the present operating point (with respect to MPP) on the P-V curve is specified to the voltage reference generator through the binary location indicator ψ. The value of ψ at the nth time instant can be calculated as follows.

$$\psi[n] \quad = \quad 1 \quad \text{if } \Gamma[n] > 0$$
$$= \quad 0 \quad \text{if } \Gamma[n] \leq 0. \tag{3.8}$$

As before, the power scarcity indicator ϕ plays the role to message convergence during the MPPT mode of operation. However, any separate convergence detection [such as (3.7)] during the LPPT mode of operation is not required.
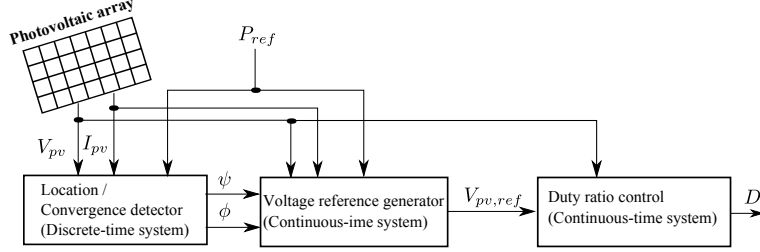
Figure 3.4: Schematic diagram of VRLPPT control.

Fig. 3.5 shows the inside view of the modified voltage reference generator in the form of block diagram. The dynamics of the voltage reference generator is, in essence, governed by the following differential equation (shown in integration form).

$$V_{pv,ref}(t) = V_{pv,ref}(0) - \int_0^t k_i^v \alpha(\tau)\sigma(\tau)d\tau. \tag{3.9}$$

Here, τ is the dummy variable representing time and t is the actual time variable. Factors σ, α and γ are defined in the same way (with μ equal to zero) as for the VSLPPT control. It is obvious that, instead of the voltage perturbation step size, the magnitude of the voltage variation rate is dynamically adjusted in this case. The base magnitude of the voltage variation rate is indicated by k_i^v. Note that the values of $\phi(t)$ and $\psi(t)$ are given by $\phi[n]$ and $\psi[n]$, respectively, for $nT_s \leq t < (n+1)T_s$. The sampling period of the location/convergence detector is indicated by T_s.
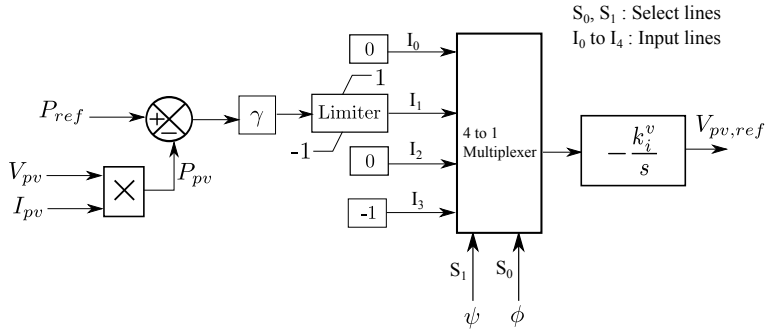
Figure 3.5: Voltage reference generator for the VRLPPT control.

Parameters T_s, k_i^v, k_p^d and k_i^d can be adjusted based upon the MPPT mode of operation. However, unlike the VSLPPT control, the parameter settings of the MPPT controller counterpart cannot be borrowed here since the architecture of the VRLPPT control is different from the architecture of the MPPT control. This, in turn, requires additional tuning effort for the VRLPPT control.

15

3.3   Simulation Results

The performances of the proposed schemes are examined through MATLAB simulations. The P&O method is employed for determining the location (with respect to MPP) of the operating point in the P-V curve. The parameters of the photovoltaic system considered for the particular study is shown in Table 3.1. A boost converter is used for the DC-DC power conversion between the photovoltaic array and the DC link. The DC link voltage is taken to be 1.52 times of the PV array open circuit voltage under STC. The parameters of different controllers are given in Table 3.2. The temperature is maintained constant throughout the simulation. Both the MPPT and LPPT modes of operation are studied. Results are produced and analyzed for different cases. Fig. 3.6 illustrates the schematic diagram of dual stage photovoltaic system connected to grid. In this chapter we are assuming DC link voltage is constant and which can be controlled by inverter [5].
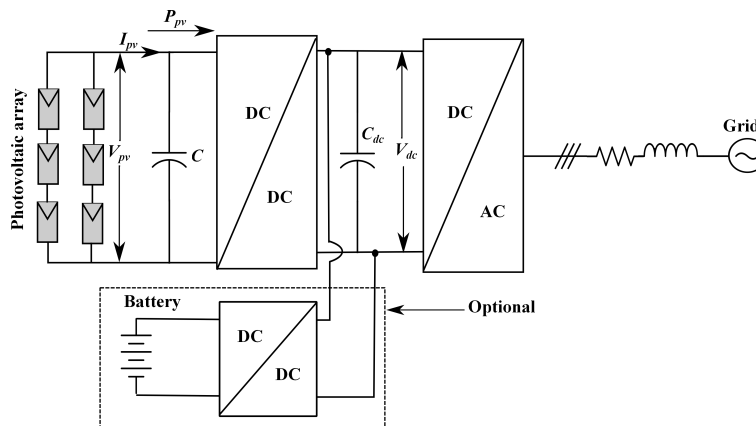
Figure 3.6: Schematic diagram of dual stage photovoltaic system.

Table 3.1: Photovoltaic system parameters

Parameter	Value
Open circuit voltage of a cell under STC	0.6093 V
Short circuit current of a cell under STC	8.21 A
Cell current temperature coefficient	0.00032 A/K
Cell voltage temperature coefficient	-0.0027 V/K
Diode ideality factor	1.3
Number of cells connected in series	540
Number of strings connected in parallel	10
Cell series resistance	0.0041 Ω
Cell parallel resistance	7.6927 Ω
Working temperature	35^0 C
Input capacitance of boost converter	0.5 mF
Boost converter inductance	9 mH
Switching frequency	2000 Hz
DC bus voltage	500 V

In order to demonstrate the effectiveness of proposed control schemes, simulations are carried out for various operating conditions. The photovoltaic system responses for different irradiance levels and power reference commands are plotted in Fig. 3.7. The system is started at t = 0 s with a

Table 3.2: DC side controller parameters

Parameter	Value
Sampling time	20 ms
Voltage step size (ΔV)	10 V
k_i^v	50 Vs^{-1}
k_p^d	0.001 V^{-1}
k_i^d	0.001 V^{-1}s^{-1}
γ (for VSLPPT)	0.0004 W^{-1}
γ (for VRLPPT)	0.1 W^{-1}
μ	0.01
ϵ	189 W (i.e., 0.01×18900)

Table 3.3: Device specifications

Device Name	Model Name	Company
eMEGAsim	OP5600	OPAL-RT
PXI	1026Q	NI

Figure 3.7: The system response for step changes in the reference power and irradiance. (a) Irradiance variation; (b) power tracking in FSLPPT; (c) power tracking in VSLPPT; (d) power tracking in VRLPPT.

reference power command of 22 kW. Initially the irradiance (G) is 1 kW/m^2. For the particular irradiance level, the maximum available power from the photovoltaic system is 18.9 kW, which is more than the reference power command. Therefore, all schemes are, initially, tracking the maximum power only with almost equal performance.

At t = 5 s, the reference power command is suddenly changed from 22 kW to 1 kW. The irradiance level remains the same. Since the new reference power command is less than the maximum available power, the LPPT mode of operation could be possible. Thus, the power output of the photovoltaic system settles down to 1 kW. The time required to make transition to the new operating point is almost the same for all the schemes. However, compared to FSLPPT, both VSLPPT and VRLPPT

17

exhibit much less oscillations at the new operating point. Minimum oscillation is observed for VRLPPT.

At t = 10 s, there is a sudden change in irradiance from 1 kW/m² to 0.5 kW/m². The maximum available power at the new irradiance level is 9.2 kW, which is still higher than the given reference power command (i.e., 1 kW). Hence, the photovoltaic system continues to operate in the limited power point tracking mode only. However, the power oscillations in FSLPPT and VSLPPT come down almost to the same level as that in VRLPPT. This is because of the lower slope of the P-V curve at the reduced irradiance level.

In another study, the photovoltaic system is initially operated under irradiance level 1 kW/m² with reference power command 15 kW. The maximum power availability corresponding to the particular irradiance level is 18.9 kW. The irradiance level is changed from 1 kW/m² to 0.5 kW/m² at t = 5 s, and reference power command is changed from 15 kW to 1 kW at t = 10 s. The maximum power availability corresponding to the irradiance level of 0.5 kW/m² is 9.2 kW. As in the previous case, VRLPPT control exhibits superiority over VSLPPT control and VSLPPT control exhibits superiority over FSLLPT control in terms of reduced power oscillation.
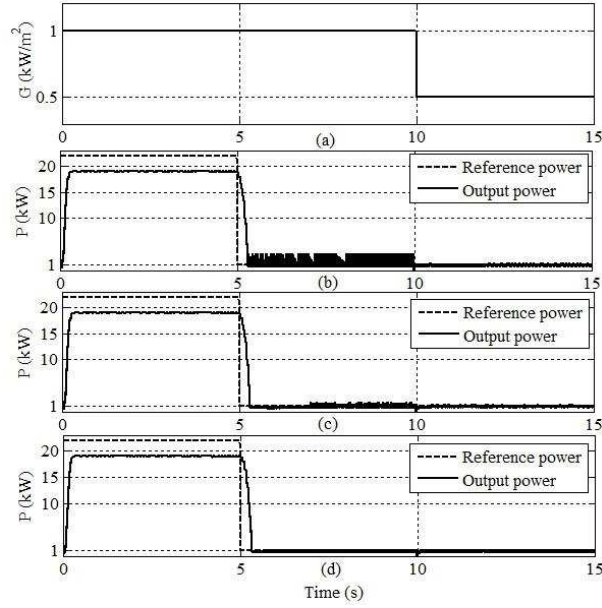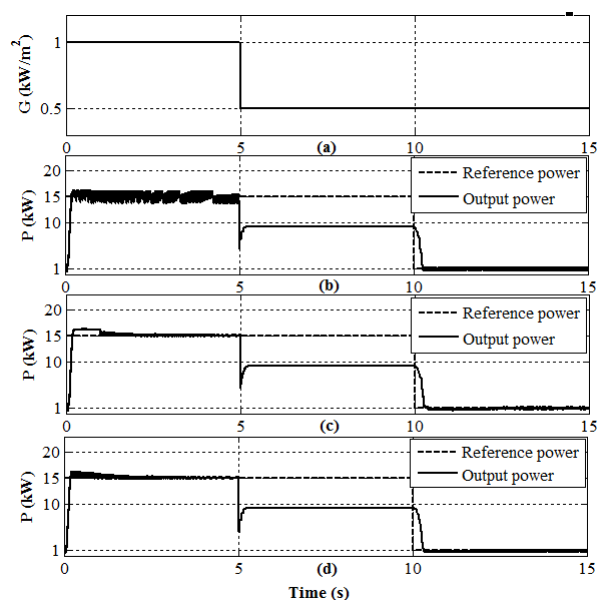

Figure 3.8: The system response for step changes in the irradiance and reference power. (a) Irradiance variation; (b) power tracking in FSLPPT; (c) power tracking in VSLPPT; (d) power tracking in VRLPPT.

3.4   HIL Setup and Results

The experimental validation of the proposed LPPT control schemes is carried out through HIL simulation. Hardware in loop simulation is a technique, which is used to test the controllers for a complex system. The HIL test setup employed is shown in Fig. 3.9. The experimental setup consists of an eMEGAsim simulator, a PXI system, a host computer, screw terminals and a port interface box. The eMEGAsim [24] and the PXI [25] are specialized computing facilities for data acquisition and real-time simulation of dynamic systems. Those are particularly useful for rapid

control prototyping to provide fast proof of concept. The description of the eMEGAsim and PXI system employed is provided in Table 3.3.
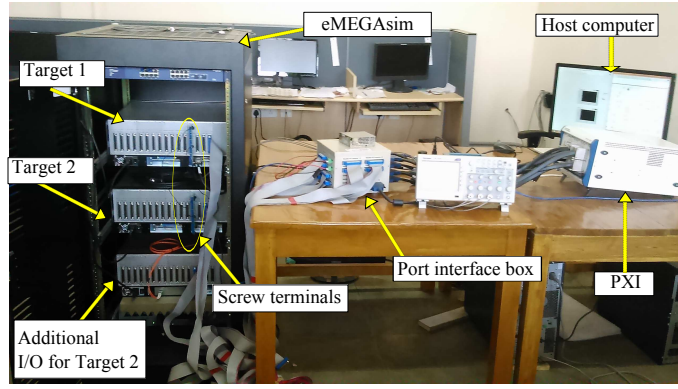
Figure 3.9: Experimental setup.
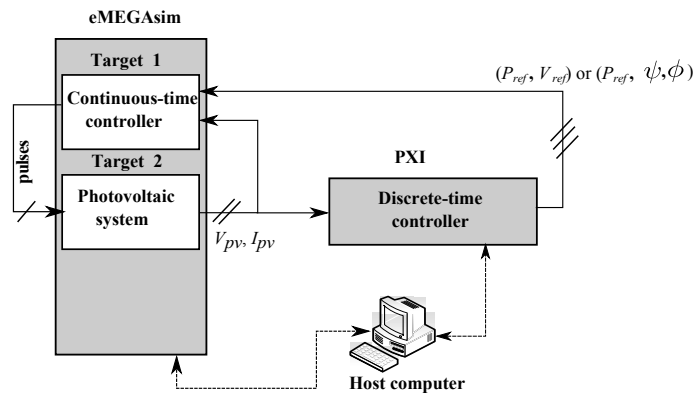
Figure 3.10: Schematic arrangement of the experimental setup.

The eMEGAsim simulator used in this experiment has two target computers (Target 1 and Target 2). Because of the unavailability of physical photovoltaic panels for the experimentation purpose, the photovoltaic system (photovoltaic array, DC-DC converter and DC link) is simulated in Target 2 of eMEGAsim. The continuous-time controller is implemented in Target 1 of eMEGAsim and the discrete-time controller is implemented in PXI. The simulations of different modules are run independently, and the interactions among different modules take place through physical (analog and digital) signals. Thus the hardware limitations in terms of measurement and sampling accuracies are taken into account. The signal exchange between Target 1 and Target 2 of eMEGAsim takes place via screw terminal connections. The signal ports of eMEGAsim are connected to the signal ports of PXI by means of FRC and NI Shielded cables via port interface box. The photovoltaic system and the continuous-time controller are modeled in RT-Lab environment. The discrete-time controller is modeled in LABVIEW. The host computer is also responsible for model loading, simulation initiation and simulation termination in eMEGAsim and PXI. The model developments are carried out in the host computer. The PXI and eMEGAsim are employed for the controller implementation since those facilities are already available with IIT Hyderabad and the concentration here is only on the proof of concept. The controllers proposed involve simple components; therefore, can easily be implemented

19

in DSP or micro-controller for the practical application.

The schematic arrangement of the experimental setup is shown in Fig. 3.10. The output voltage and current measured from the photovoltaic system module are fed to both continuous-time and discrete-time controllers. Based on that input, the discrete-time controller generates the reference voltage for the VSLPPT (or FSLPPT) control or location and power scarcity indicators for the VRLPPT control. The reference power command is provided to the discrete-time controller and is subsequently passed to the continuous-time controller. Based upon the inputs from photovoltaic system and discrete-time controller modules, switching pulses are generated by the continuous-time controller. The pulses generated are fed to the DC-DC converter of the photovoltaic module running in Target 2.

Figure 3.11: Experimental results showing output power variation of the photovoltaic system for decrease in irradiance from 1 kW/m^2 to 0.5 kW/m^2 at reference power 15 kW. (a) FSLPPT method; (b) VSLPPT method; (c) VRLPPT method.

The output voltage ranges (analog signals) of eMEGAsim and PXI are -16 V to +16 V and -10 V to +10 V, respectively. Therefore, all the quantities to be exchanged between different modules are scales down to -9.5 V to +9.5 V. The scaling factors employed are chosen according to the panel
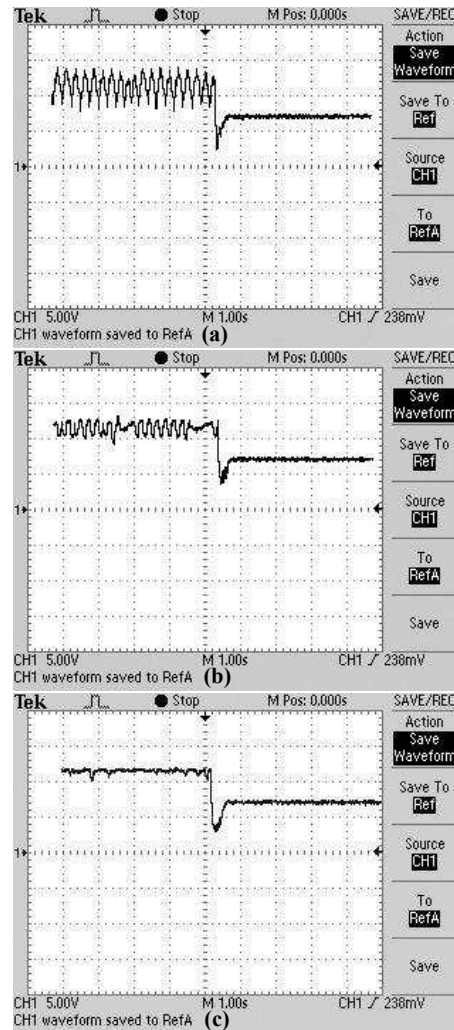
Figure 3.12: Experimental results showing output power variation of the photovoltaic system for increase in irradiance from 0.5 kW/m^2 to 0.8 kW/m^2 at reference power 15 kW. (a) FSLPPT method; (b) VSLPPT method; (c) VRLPPT method.

rating. For this particular experiment, the scaling factors for voltage, current and power are selected as 0.019, 0.095 and 0.000475, respectively. Pulses, location indicator and power scarcity indicator are provided in the form of 0 V or 5 V signals.

Experiments are carried out for irradiance levels 1 kW/m^2, 0.8 kW/m^2 and 0.5 kW/m^2. The corresponding maximum power availabilities is 18.9 kW, 15.1 kW and 9.2 kW, respectively. Different power reference commands provided are 20 kW, 15 kW and 2 kW, respectively. The responses of the photovoltaic system to the varying environmental condition and reference power command are observed both for the prospective increase and decrease in the power output. Similarly, the transition between LPPT to MPPT, modes in either way is verified. The first set of results is obtained for a sudden decrease in irradiance from 1 kW/m^2 to 0.5 kW/m^2 under the reference power command of 15 kW. The corresponding results are plotted in Fig. 4.4. For this case, the operation of the photovoltaic system shifts from the LPPT mode to the MPPT mode with reduction in power output. For the second case, the irradiance is suddenly increased from 0.5 kW/m^2 to 0.8
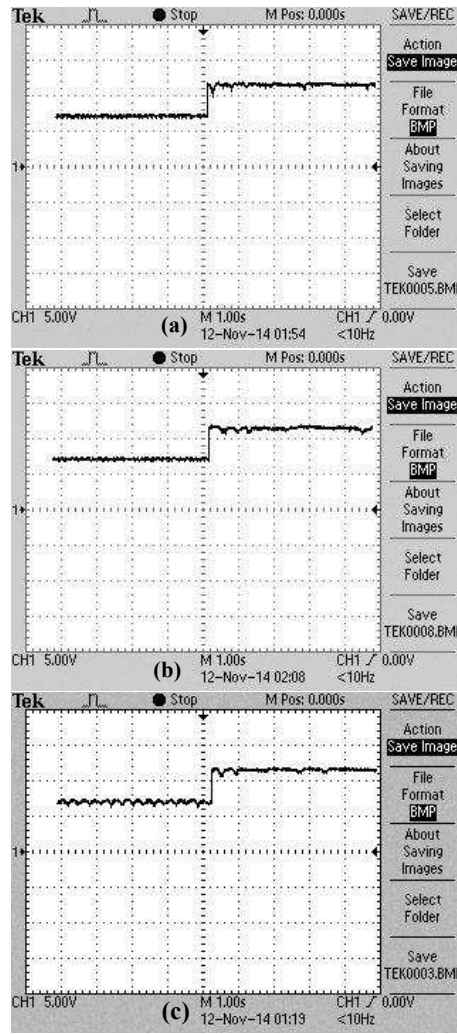
21
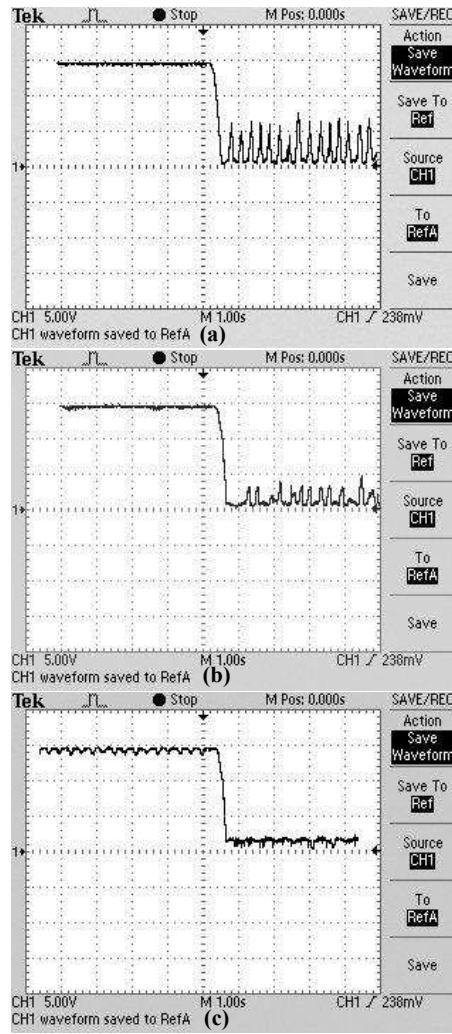
Figure 3.13: Experimental results showing output power variation of the photovoltaic system for decrease in reference power from 20 kW to 2 kW at the irradiance 1 kW/m^2. (a) FSLPPT method; (b) VSLPPT method; (c) VRLPPT method.

kW/m^2. The same power reference command, as in the previous case, is applied. Here, the power output of the photovoltaic system increases although the mode of operation continues being MPPT only. The results for the second case are plotted in Fig. 4.5. The third and fourth cases consider sudden variations of the reference power command under a fixed irradiance level (which is set to 1 kW/m^2). For the third case, reference power command is suddenly decreased from 20 kW to 2 kW, whereas, for the fourth case, the power reference command is suddenly increased from 15 kW to 20 kW. The corresponding results are shown in Fig. 4.6 and Fig. 4.7, respectively. The system reacts to the above mentioned increase and decrease in the reference power command by increasing and decreasing its power output, respectively. When the reference power command is reduced, the LPPT mode of operation is assumed after departing from the initial MPPT mode. The reverse is the case where the power reference command is increased. It is to be noted that, in all the oscilloscope generated plots, the time scale is 1 s/division and the power scale is 6.67 kW/division.

From the above results, it is obvious that all the schemes correctly respond to the variations
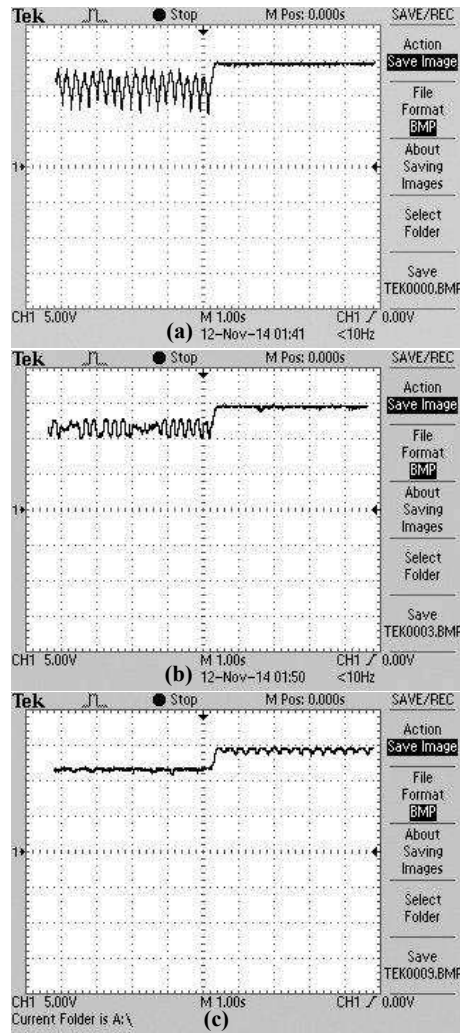
Figure 3.14: Experimental results showing output power variation of the photovoltaic system for reference power increase from 15 kW to 20 kW at irradiance 1 kW/m^2. (a) FSLPPT method; (b) VSLPPT method; (c) VRLPPT method.

in environmental condition and reference power command. For all the cases, transition to the new operating point takes place in less than 0.7 s. However, there is, sometimes, additional delay (compared to the existing method) of around 0.1 s in the response times of the proposed schemes. The amount of oscillation that is found in the existing method during the LPPT operation (i.e., when the power production is less than the maximum available power) is always quite high. The improvement in the LPPT performance is moderate under the VSLPPT control and significant under the VRLPPT control. However, in the case of VRLPPT control, slightly more oscillation is seen in most of the cases during maximum power point tracking. It is to be mentioned that the right half portion of Fig. 4.4(c) should have been identical to that of the left half portion of Fig. 4.5(c) (since both correspond to the same operating condition). The slight difference is found to happen because of the extended time of simulation of the MPPT operation in Fig. 4.5.

23

3.5   Conclusions

In this chapter, two novel control schemes are proposed for the precise and stable limited power point tracking of a photovoltaic plant. A dual stage photovoltaic system configuration with DC bus voltage being controlled by battery converter or DC-AC converter is considered. Unlike the existing FSLPPT control, the LPPT control techniques proposed exhibit fewer oscillations at low power levels with almost the same response time. The proposed VSLPPT control employs a variant form of the conventional MPPT algorithms with variable perturbation step size. The step size is adjusted in proportion to the absolute value of the difference between the reference power and the actual output power, but is capped at some upper limit. The upper limit is implemented to get satisfactory MPPT performance when the specified reference power level is higher than the maximum available power. The VSLPPT scheme performs better than the existing method at all power levels and is quite simple. The other LPPT control scheme proposed (called as VRLPPT) employs an additional continuous-time controller, but is based upon the uniform variable step size concept as is employed in the VSLPPT control. The performance of the VRLPPT control is far superior to the performance of the FSLPPT or VSLPPT control at low power levels. The particular superiority in performance happens because of conceptually employing infinitesimally small perturbation step sizes in the VRLPPT control. However, slightly more oscillations are observed near the maximum power point.

Chapter 4

Limited Power Control of Single Stage Grid Connected Photovoltaic System

Nowadays, single-stage grid connected systems are gaining more popularity than dual stage grid connected systems. Single-stage operation has higher efficiency and lower cost compared to dual-stage grid connected operation. In this chapter, the performance of LPPT by using FSLPPT control is studied for a three phase single-stage grid connected photovoltaic system.

4.1 Structure of Single-Stage Photovoltaic System

Fig. 4.1 presents the schematic representation of a single-stage photovoltaic system connected to the grid. In this configuration, photovoltaic array delivers power to the grid directly through a voltage source converter (VSC). The responsibility of the VSC is to control the DC link voltage to the reference level. The DC link voltage control is achieved through a DC link voltage controller and a current controller that are shown in Fig. 4.2 and Fig. 4.3, respectively [5]. Here, the d-q transformation is performed with the convention that the q-axis leads the d-axis and the reference frame angle is defined by the position of the d-axis. Based upon the deviation of the DC link voltage (symbolized as V_{dc}) from the reference level (symbolized as V_{dcref}), the DC link generates a reference signal for the d-component of the filter inductor current. The reference value for the q-component of the filter inductor current can be independently specified. In this chapter, i_{qref} is taken to be zero for the unity power factor operation of the VSC. Based upon the current reference commands, the current controller generates modulation signals the VSC to draw the necessary amount of power from the DC side. The $abc - dq$ transformation matrix employed is shown in 4.1.

In the case of dual-stage photovoltaic power conversion, the DC link reference voltage is kept constant. The voltage output of the photovoltaic array is regulated by a DC-DC converter. However, in the case of single-stage photovoltaic power conversion, the DC link voltage also indicates the photovoltaic array output voltage. Therefore, the voltage reference command to the DC link voltage controller should vary according to the amount of power to be drawn from the photovoltaic array.

25

The reference value for the DC link voltage is determined by the LPPT controller according to the specified reference power level P_{ref}.

$$
\begin{bmatrix} f_a \\ f_b \\ f_c \end{bmatrix} = \sqrt{\frac{2}{3}} \begin{bmatrix} \cos\theta & -\sin\theta & \frac{1}{\sqrt{2}} \\ \cos(\theta - \frac{2\pi}{3}) & -\sin(\theta - \frac{2\pi}{3}) & \frac{1}{\sqrt{2}} \\ \cos(\theta + \frac{2\pi}{3}) & -\sin(\theta + \frac{2\pi}{3}) & \frac{1}{\sqrt{2}} \end{bmatrix} \begin{bmatrix} f_d \\ f_q \\ f_0 \end{bmatrix}
\tag{4.1}
$$

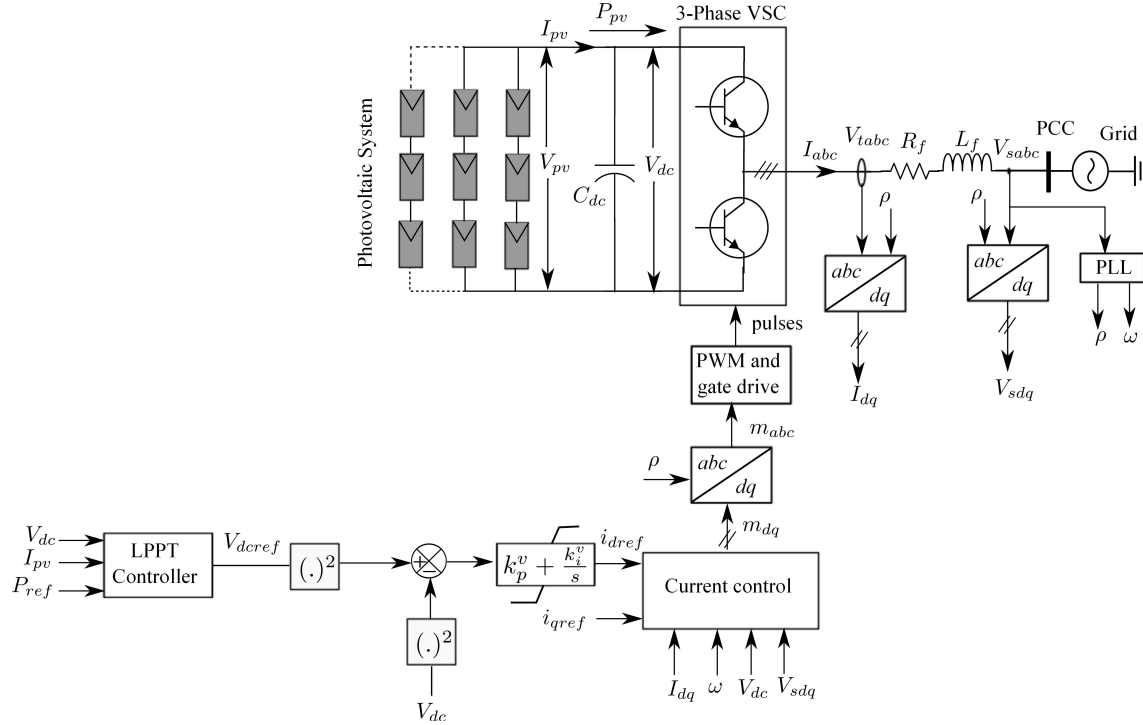Figure 4.1: Schematic diagram of a single-stage photovoltaic system connected to grid.

4.1.1 DC link Voltage Controller

The block diagram for the DC link voltage controller is shown in Fig. 4.2. The main purpose of DC link voltage controller is regulate the DC link voltage to reference voltage (V_{dcref}), which, in turn, is determined by LPPT scheme [5].
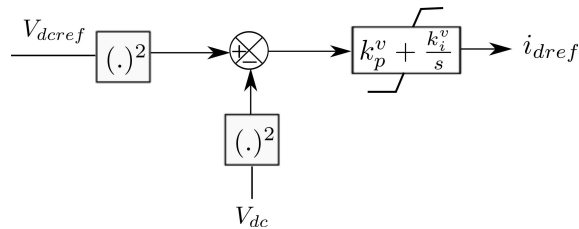

Figure 4.2: Block diagram of DC-link voltage controller.

26

4.1.2 Current Controller

The block diagram for the DC link voltage controller is shown in Fig. 4.3. The current control scheme, is to regulate the d and q axis components of filter current i_{abc} [5].
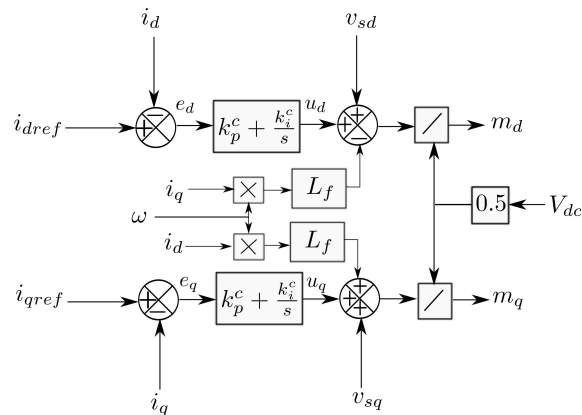

Figure 4.3: Block diagram of current controller.

4.2 Simulation Results

Simulation studies are carried out under MATLAB/SIMULINK environment. The photovoltaic array is modelled by means of the equations shown in [5] and [27]. The current controller parameters are tuned by following the procedure explained in [26]. The LPPT controller and DC link voltage controller parameters are tuned by trial and error method according to the maximum power tracking performance at standard test condition. Four different cases of rapid variation in operating conditions are studied. The temperature is kept constant at 35^0 C throughout the simulation. Photovoltaic system parameters is presented in Table 3.1, and control parameters are presented in Table 4.1 to Table 4.3.

Table 4.1: System parameters

Photovoltaic System Parameter	Value
Number of cells connected in series	1620
Number of strings connected in parallel	10
DC link capacitance	0.5 mF
Switching frequency	2550 Hz

Table 4.2: Grid and AC side filter parameters

Grid and AC side filter parameters	Value
Grid voltage	400 V (rms L-L)
Grid frequency	50 Hz
L_f	6.71 mH
R_f	0.295 Ω

Table 4.3: AC side controller parameters

AC side controller parameters	Value
Voltage step size (ΔV)	10 V
k_p^c	6.71 Ω
k_i^c	295 Ωs^{-1}
k_p^v	-0.01 A/V^2
k_i^v	-0.008 As^{-1}/V^2
ϵ	0

4.2.1 Case 1: Step Increase in Reference Power Command

In this case, the transition from LPPT mode to MPPT mode because of a sudden increase of reference power command is verified. The irradiance level is maintained constant at 1 kW/m^2. The maximum power available corresponding to the particular irradiance level is 60.2 kW. The system is primarily operated with a reference power command 40 kW. It is possible to track this reference power level because of adequate power available. At t = 2 s, the reference power command is suddenly increased to 62 kW. Since the new reference power command exceeds maximum power available, the system can operate only at the maximum power point. Results for the photovoltaic array power output, DC link voltage and VSC output currents are plotted in Fig. 4.4. It can be observed that the transition from the LPPT mode to the MPPT mode take place successfully within around 0.5 s. There are some oscillations during the LPPT mode of operation. This is due to the steep slope of the P-V curve at the right hand side of MPP. Although the new reference power command cannot be tracked, the power output of the photovoltaic array still increases. This in turn results in reduction of the DC link voltage because of the inverse relationship between power and voltage in the operating zone.
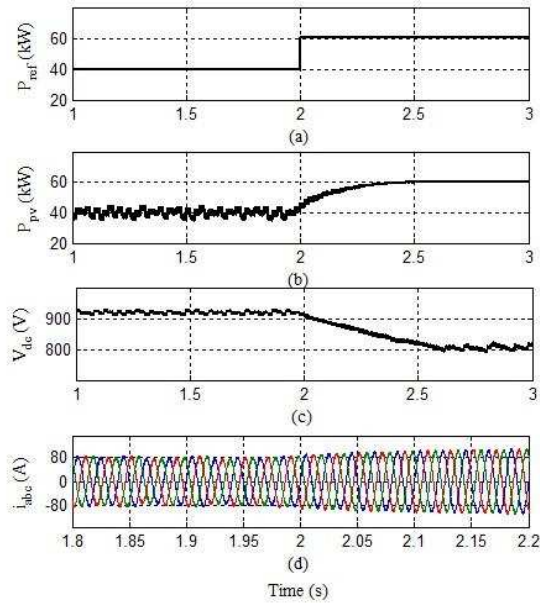

Figure 4.4: Photovoltaic system response for step increase in reference power command. (a) Reference power; (b) photovoltaic array power output; (c) DC link voltage; (d) VSC output current.

28

4.2.2 Case 2: Step Decrease in Reference Power Command

In this case, the transition from MPPT mode to LPPT mode because of the sudden decrease of reference power command is verified. The same irradiance level as in the previous case is retained. The system has originally operated with a reference power command 62 kW. At t = 2 s, the reference power command is suddenly decreased to 50 kW. Fig. 4.5 shows a successful transition from the MPPT mode to the LPPT mode within around 0.3 s. The decrease in the power output of the photovoltaic array leads to higher DC link voltage.
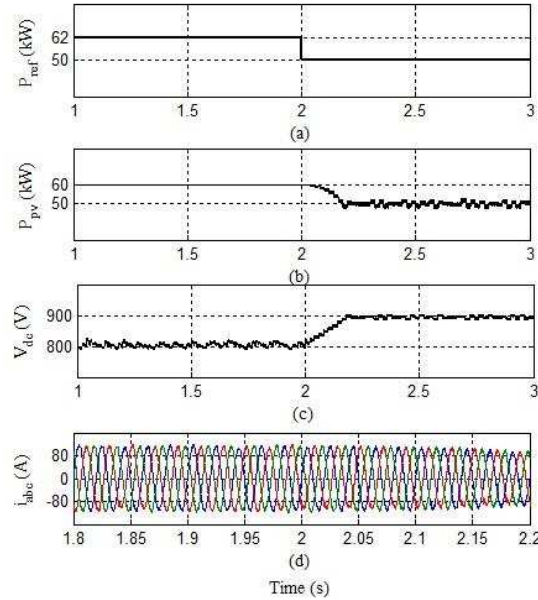

Figure 4.5: Photovoltaic system response for step decrease in reference power command. (a) Reference power; (b) photovoltaic array power output; (c) DC link voltage; (d) VSC output current.

4.2.3 Case 3: Step Increase in Irradiance level

In this case, the transition from LPPT mode to MPPT mode because of a sudden decrease in irradiance level is verified. The power reference command is set fixed at 50 kW. The initial irradiance level is taken as 1 kW/m^2. The maximum power available corresponding to the particular irradiance level is 60.2 kW indicating power adequacy to meet the specified power requirement. At t = 2 s, the irradiance level, suddenly comes down to 0.8 kW/m^2. As a consequence, the maximum power available also gets reduced to 47.3 kW resulting in power deficiency. As is shown in Fig. 4.6, the mode of operation of the photovoltaic system correctly shifts from LPPT to MPPT. The time required for this transition to happen is around 0.3 s.

4.2.4 Case 4: Step Decrease in Irradiance level

In this case, the transition from MPPT mode to LPPT mode because of a sudden increase in irradiance level is verified with the same reference power command as before. The irradiance level is suddenly increased from 0.8 kW/m^2 to 0.9 kW/m^2 at t = 2 s. Fig. 4.7 depicts the mode transition. The mode transition takes place within 0.2 s.
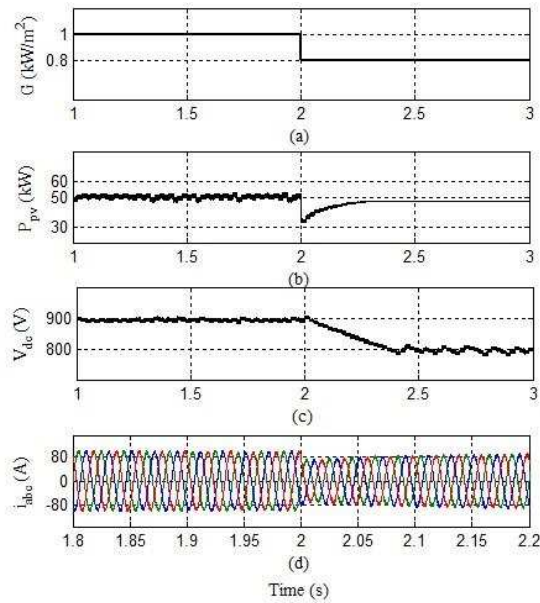
Figure 4.6: Photovoltaic system response for step decrease in irradiance level. (a) Irradiance; (b) photovoltaic array power output; (c) DC link voltage; (d) VSC output current.
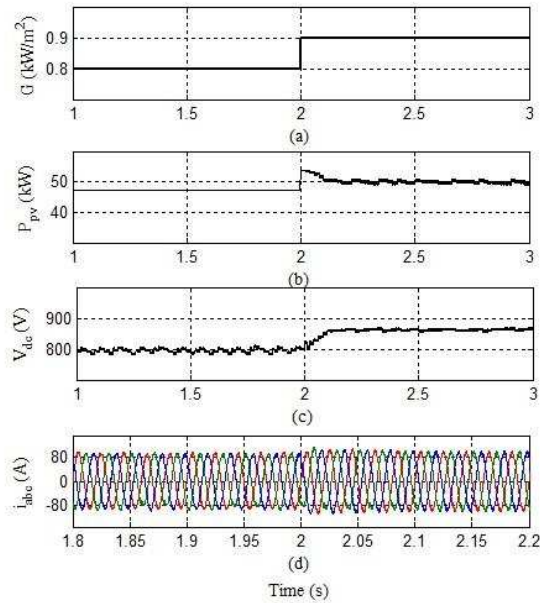
Figure 4.7: Photovoltaic system response for step increase in irradiance level. (a) Irradiance; (b) photovoltaic array power output; (c) DC link voltage; (d) VSC output current.

4.3   Experimental Results

The performance of LPPT control for single stage photovoltaic power conversion is verified by a HIL experiment. The experimental setup is shown in Fig. 3.9. Single line diagram of the experimental setup is shown in Fig. 4.8. Photovoltaic system, inverter and grid are simulated in Target 1. The

current controller, the DC link voltage controller and the pulse width modulation (PWM) controller (together called as continuous time controller) of the DC-AC converter are deployed in Target 2. LPPT controller (i.e., discrete time controller) is implemented in PXI. All the simulations will run independently. The LPPT controller is modelled in LABVIEW. The Photovoltaic system, inverter and continuous time controller is modelled in RT-LAB.
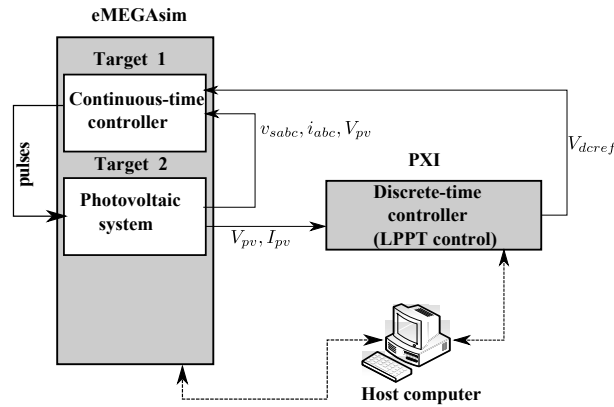
Figure 4.8: Single line diagram of the experimental setup.
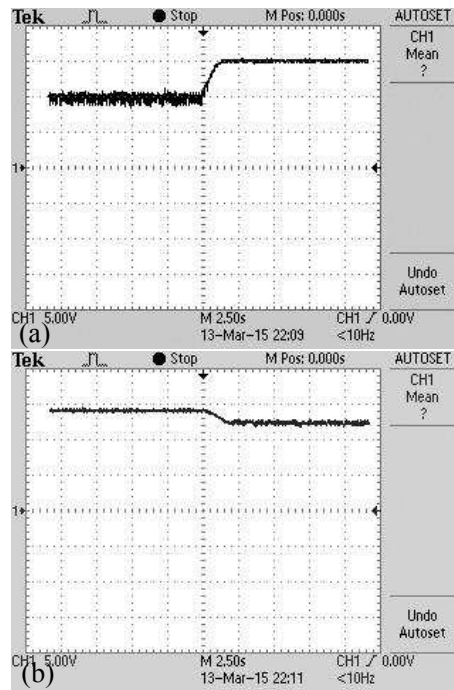
Figure 4.9: Experimental results corresponding to reference power increase from 40 kW to 62 kW. (a) Photovoltaic array power output; (b) DC link voltage. Y-axis scale: 4133.33 W/div, 66.67 V/div. X-axis scale: 5 s/div.
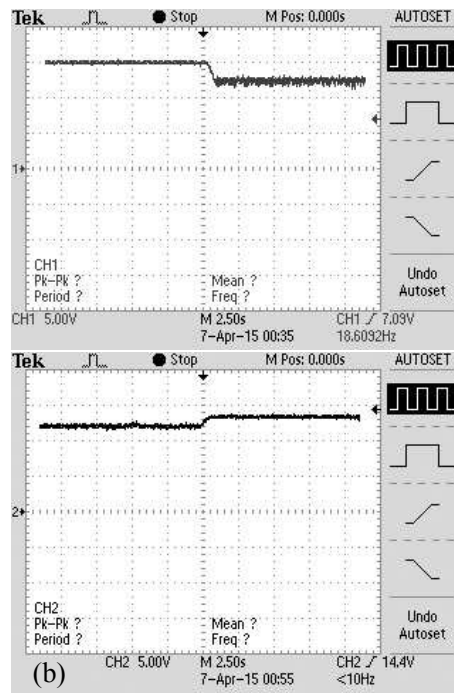
Figure 4.10: Experimental results corresponding to reference power decrease from 62 kW to 50 kW. (a) Photovoltaic array power output; (b) DC link voltage. Y-axis scale: 4133.33 W/div, 66.67 V/div. X-axis scale: 5 s/div.

Figure 4.11: Experimental results corresponding to irradiance decrease from 1 kW/m^2 to 0.80 kW/m^2. (a) Photovoltaic array power output; (b) DC link voltage. Y-axis scale: 4133.33 W/div, 66.67 V/div. X-axis scale: 5 s/div.

Figure 4.12: Experimental results corresponding to irradiance increase from 0.80 kW/m² to 0.90 kW/m². (a) Photovoltaic array power output; (b) DC link voltage. Y-axis scale: 4133.33 W/div, 66.67 V/div. X-axis scale: 5 s/div.
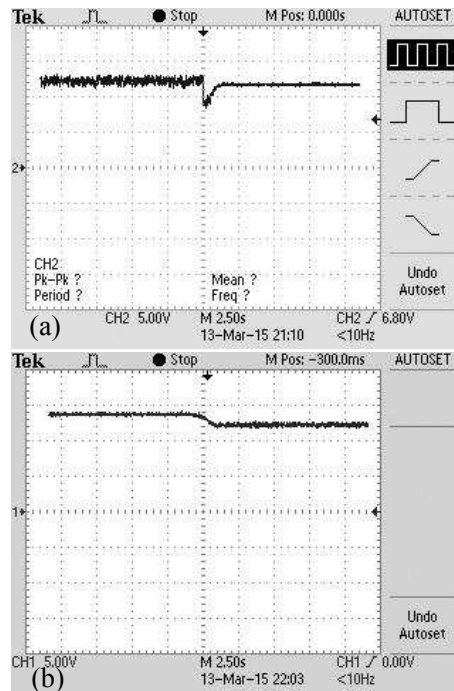
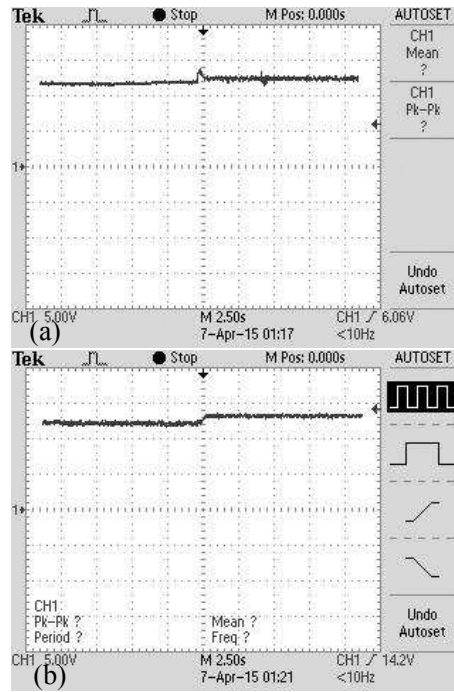## 4.4 Conclusions

This chapter is a study on the LPPT control of single stage, three-phase grid connected photovoltaic system. In the case of a single stage photovoltaic system, the photovoltaic array is directly interfaced with the grid through a DC-AC converter. Therefore, the output voltage of the photovoltaic array (and, thus, the photovoltaic power output) is controlled by the DC-AC converter itself. The LPPT control over a single stage photovoltaic system can be performed in the similar way as that in the MPPT control. The LPPT controller employed is, in effect, a variant version of the conventional MPPT controller. However, in the case of LPPT control, the inverter is exposed to larger variation in its input voltage. Detailed simulation and experimental, studies are performed to verify the tolerance of the DC-AC converter to such large input variation. The experimental study is carried out by means of HIL simulations with eMEGAsim and PXI systems. Different cases of operation condition are considered. For all the cases, stable system performance is noted. However, as usual, there may be some power oscillations at low power levels.

Chapter 5

Summary and Future Work

5.1 Summary

The objective of this thesis is to improve the performance of LPPT of photovoltaic plants. The previously reported LPPT methods, however, exhibit more oscillations at low power levels or require additional mode changing action. To avoid those difficulties, two novel LPPT control schemes are proposed. A dual stage photovoltaic system configuration with DC bus voltage being controlled by battery converter or DC-AC converter is considered. The control schemes proposed are called as VSLPPT control and VRLPPT control, respectively. Both the schemes are carefully designed with minimum deviation from the traditional MPPT control so as to ensure easy implementation. Unlike the existing FSLPPT control, the LPPT control techniques proposed exhibit fewer oscillations at low power levels with almost the same response time. The proposed VSLPPT control employs a variant form of the conventional MPPT algorithms with variable perturbation step size. The step size is adjusted in proportion to the absolute value of the difference between the reference power and the actual output power, but is capped at some upper limit. The upper limit applies to get satisfactory MPPT performance when the specified reference power level is higher than the maximum available power. The VSLPPT scheme performs better than the existing method at all power levels and is quite simple. The other LPPT control scheme proposed (called as VRLPPT) employs an additional continuous-time controller, but is based upon the uniform variable step size concept as is employed in the VSLPPT control. The performance of the VRLPPT control is far superior to the performance of the FSLPPT or VSLPPT control at low power levels. The actual superiority in performance happens because of conceptually employing infinitesimally small perturbation step sizes in the VRLPPT control. However, slightly more oscillations are observed near the maximum power point. The proposed LPPT control schemes are tested under different conditions, and their performances are thoroughly verified.

This thesis also presents a study on the LPPT control of single-stage, three-phase grid connected photovoltaic system. In the case of a single-stage photovoltaic system, the photovoltaic array is directly interfaced with the grid through a DC-AC converter. The experimental study is carried out by means of HIL simulations with eMEGAsim and PXI systems. Different cases of operating conditions are considered.

5.2   Future Work

The following topics are suggested for future work.

- Hardware implementation of LPPT for grid connected PV system.

- Generation of reference power command based on the frequency deviation (from the reference frequency).

- Modification of LPPT control according to the partial shading conditions.

- Design of LPPT controls for islanded mode of operation.

References

[1] Y. Yang, H. Wang, F. Blaabjerg, and T. Kerekes, "A hybrid power control concept for PV inverters with reduced thermal loading," *IEEE Trans. Power Electron.,* vol. 29, no. 12, pp. 6271–6275, May. 2014.

[2] R. Tonkoski, L. A. C. Lopes, and T. H. M. El-Fouly, "Coordinated active power curtailment of grid connected PV inverters for overvoltage prevention," *IEEE Trans. Sustain. Energy,* vol. 2, no. 2, pp. 139–147, Apr. 2011.

[3] NREL. (2013, Sep.). *Variable renewable generation can provide balancing control to the electric power system* [Online]. Available: http://www.nrel.gov/docs/fy13osti/57820.pdf.

[4] L. D. Watson and J. W. Kimball, "Frequency regulation of a microgrid using solar power," in *Proc. Appl. Power Electron. Conf. and Expo.,* Mar. 2011, pp. 321–326.

[5] A. Yazdani, A. R. Di Fazio, H. Ghoddami, M. Russo, M. Kazerani, J. Jatskevich, K. Strunz, S. Leva, and J. A. Martinez, "Modeling guidelines and benchmark for power system simulation studies of three phase single stage photovoltaic systems," *IEEE Trans. Power Del.,* vol. 26, pp. 1247–1264, Apr. 2011.

[6] M. G. Villava, J. R. Gazoli, and E. R. Filho, "Comprehensive approach to modelling and simulation of photovoltaic arrays," *IEEE Trans. Power Electron.,* vol. 24, no. 5, pp. 1198–1208, May. 2009.

[7] A. Yazdani and P. P. Dash, "A control methodology and characterization of dynamics for a photovoltaic (PV) system interfaced with a distribution network," *IEEE Trans. Power Del.,* vol. 24, no. 3, pp. 1538–1551, Jul. 2009.

[8] W. Xiao, W. G. Dunford, P. R. Palmer, and A. Capel, "Regulation of photovoltaic voltage," *IEEE Trans. Power Electron.,* vol. 54, no. 3, pp. 1365–1374, Jun. 2007.

[9] F. Blaabjerg, F. Iov, T. Kerekes, and R. Teodorescu, "Trends in power electronics and control of renewable energy systems," in *Proc. Power Electron. and Motion Control Conf.,* Sep. 2010, pp. 6–8.

[10] S. B. Kjaer, J. K. Pedersen, and F. Blaabjerg, "A review of single-phase grid-connected inverters for photovoltaic modules ," *IEEE Trans. Ind. Applicat.,* vol. 41, no. 5, pp. 1292–1306, Sep.-Oct. 2005.

[11] T. Esram and P. L. Chapman, "Comparison of photovoltaic array maximum power point tracking techniques," *IEEE Trans. Energy Convers.,* vol. 22, no. 2, pp. 434–449, Jun. 2007.

[12] T. Esram, J. W. Kimball, P. T. Krein, P. L. Chapman, and P. Midya, "Dynamic maximum power point tracking of photovoltaic arrays using ripple correction control," *IEEE Trans. Power Electron.,* vol. 21, no. 5, pp. 1282–1291, Sep. 2006.

[13] Y. Yang, F. Balaabjerg, and H. Wang, "Constant power generation of photovoltaic systems considering the distributed grid capacity," in *Proc. IEEE Applied Power Electron. Conf. and Expo.,* Mar. 2014, pp. 379–385.

[14] A. Hoke and D. Maksimovic, "Active power control of photovoltaic power systems," in *Proc. IEEE Conf. Technologies for Sustainability,* 2013, pp. 70–77.

[15] H. Asano, K. Yajima, and Y. Kaya, "Influence of photovoltaic power generation on required capacity for load frequency control," *IEEE Trans. Energy Convers.,* vol. 11, no. 1, pp. 188–193, Mar. 1996.

[16] V. A. K. Pappu, B. H. Chowdary, and R. Bhatt, "Implementing frequency regulation capability in a solar photovoltaic power plant," in *Proc. North Amer. Power Symp.,* Sep. 2010, pp. 26–28.

[17] O. Alizadeh and A. Yazdani, "A strategy for real power control in a direct-drive PMSG-based wind energy conversion system," *IEEE Trans. Power Del.,* vol. 28, no. 3, pp. 1297–1305, Jul. 2013.

[18] N. Bhugra and K. P. Detroja, "Sliding mode control based power balancing for grid connected PV system," in *Proc. IEEE Int. Conf. Control Applicat.,* Aug. 2013, pp. 673–678.

[19] A. Urtasun, P. Sanchis, and L. Marroyo, "Limiting the power generated by photovoltaic system," in *Proc. Int. Multi-Conf. Syst. Signals and Devices*, Mar. 2013, pp. 1–6.

[20] S. M. Park and S. Y. Park, "Power weakening control of the photovoltaic battery system for seamless energy tranfer in microgrids," in *Proc. Appl. Power Electron. Conf.,* Mar. 2013, pp. 2971–2976.

[21] A. Ahmed, L. Ran, S. Moon, and J. H. Park, "A fast PV power tracking control algorithm with reduced power mode," *IEEE Trans. Energy Convers.,* vol. 28, no. 3, pp. 565–575, Sep. 2013.

[22] P. P. Zarina, S. Mishra, and P. C. Sekhar, "Photovoltaic system based transient mitigation and frequency regulation," in *Proc. Annu. IEEE India Conf.,* 2012, pp. 1245–1249.

[23] F. Liu, S. Duan, F. Liu, B. Liu, and Y. Kang, "A variable step size INC MPPT method for PV systems," *IEEE Trans. Ind. Applcat.,* vol. 55, no. 7, pp. 2622–2628, Jul. 2008.

[24] [Online]. Available: http://www.opal-rt.com/product/emegasim-powergrid-real-time-digital-hardware-in-the-loop-simulator.

[25] [Online]. Available: http://www.ni.com/data-acqusition.

[26] A. Yazdani and R. Iravani, *Voltage-Sourced Converters in Power Systems.* Piscataway, NJ: IEEE/Wiley, 2010.

[27] M. B. Delghavi and A. Yazdani, "A control strategy for islanded operation of a distributed resource (DR) unit," in *Proc. IEEE Power Engineering Society General Meeting,* Jul. 2009, pp. 26–30.